

AN INVESTIGATION OF BACKSCATTER POWER SPECTRA FROM CELLS, CELL PELLETS AND MICROSPHERES

M.C. Kolios^{1,2}, L. Taggart^{2,3}, R..E. Baddour^{1,2}, F.S. Foster^{2,4}, J.W. Hunt^{2,3}, G.J. Czarnota^{1,3} and M.D. Sherar^{2,3}

¹Dept. of Mathematics, Physics and Computer Science, Ryerson University, Toronto, ON, M5B2K3, Canada,

²Dept. of Medical Biophysics, University of Toronto, 610 University Avenue, Toronto, ON, M5G2M9, Canada

³Ontario Cancer Institute, Princess Margaret Hospital, 610 University Avenue, Toronto, ON, M5G2M9, Canada

⁴Imaging Physics, Sunnybrook and Women's College Health Sciences Centre, Toronto ON, M4N 3M5, Canada

Abstract – It has been previously shown that high frequency ultrasound (20 - 100 MHz) can be used to detect cellular structure changes in tissues and cell ensembles. However, the changes seen in the backscattered ultrasound intensity and frequency spectrum are not fully understood. In this paper we attempt to better understand the nature of these changes by examination of the backscatter power spectra from cell ensembles (in pellet form) that have undergone two different types of cell death: by exposure to the chemotherapeutic cisplatin and by withdrawal of nutrients (decay). Three different ultrasound transducers were used, centered at 20MHz and 40MHz. In both death pathways, an increase of the midband fit of 10-12dB was measured, and there were significant changes in the spectral slopes. Furthermore, our initial analysis of the backscatter from single cells and polystyrene microspheres demonstrates the potential of the technique to assess scatterer size.

I. INTRODUCTION

In previous publications[1, 2], we have shown that the backscatter from cell ensembles treated with the chemotherapeutic cisplatin (thus inducing apoptosis in those experiments) increased the ultrasound backscatter by 9-13dB and produced changes in the normalized frequency spectrum. The most striking histological features in the treated cells were the nuclear condensation, the cell shrinkage and membrane disruption. However, we have not yet understood the nature of the backscatter increase and the subtle changes in power spectra[3]. Changes in the backscatter are due to changes in the size, concentration, acoustic impedance and spatial

distribution of the ultrasound scatterers, all of which may be modified during these experiments. In this work, we repeat the experiments using a 20MHz and 40MHz transducer to examine whether these changes can be imaged at lower frequencies. We leave cells in a pellet to decay (thus emulating oncotic necrosis) and examine the changes in the ultrasound backscatter and power spectra. Finally, the backscatter from single cells and polystyrene microspheres of the same size were compared to obtain a better understanding of the backscattering process at these frequencies and scales.

II. IMAGING CELL PELLETS: EXPOSURE OF CELLS TO TOXIC DRUG

Data were collected from cell pellets to examine whether the changes in ultrasound backscatter previously observed after treating Acute Myeloid Leukemia (AML) cells with the chemotherapeutic cisplatin could be detected at lower frequencies making the technique of detecting cell damage more relevant to clinical ultrasound frequencies. To this end, two broadband transducers were used to image cell pellets: one with a center frequency of 20MHz (8.5mm diameter, f2.3, -6dB bandwidth: 12-30MHz) and the other 40MHz (3mm diameter, f2, -6dB bandwidth: 20-53MHz). The transducers were purchased from VisualSonics Inc. (www.visualsonics.com) and attached to the VS40B ultrasound imager. The VS40B has the ability to select regions of interest from the B-scan images and store the raw radio-frequency (rf) data associated with the region of interest (ROI). Apart from the better SNR, the system has enabled us to make more precise measurements compared to the old scanner by

reducing data acquisition time (thus collecting more data for averaging).

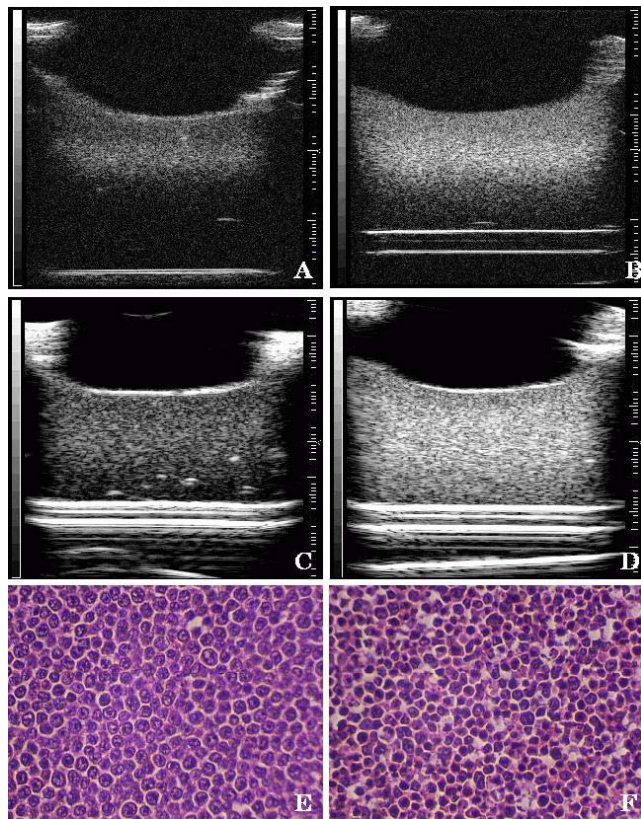


Figure 1: Ultrasonic B-mode images of AML cell pellets (8x8mm) imaged at 40MHz (A and B) and 20MHz (C and D). Ultrasonic images of the untreated cells are shown in panels A and C, with the corresponding H&E histology in panel E. Ultrasonic images of the treated cells (24h exposure) are shown in panels B and D with the corresponding H&E histology in panel F.

The methodology of the biological experiments can be found elsewhere[1]. Briefly, cells were prepared using a cell culture system. Approximately 10^9 human acute myeloid leukemia cells were grown at 37°C in α -minimal-media from frozen stock sample using 150ml of media and treated with cisplatin at a concentration of 10 $\mu\text{g}/\text{ml}$. Cells were washed in phosphate-buffered saline and the preparations were subsequently pelleted in flat bottom plastic tubes on a swinging bucket centrifuge. After the ultrasound data collection, pellets were fixed for Haematoxylin and Eosin staining or electron microscopy. A new technique was developed by which the cells were fixed and stained as a solid pellet, thereby enabling examination of the distribution of cells.

Representative ultrasound images are shown in Figure 1. Panels A and B show B-scan images using the 40MHz f2 transducer (focus $\sim 1\text{mm}$ below pellet surface). There is a marked increase in backscatter, the mid-band fit (which is analogous to the integrated backscatter[4]) increasing by $\sim 11\text{dB}$, consistent with our previous studies[2]. A similar increase in ultrasound backscatter is also measured with the 20MHz f2.3 transducer (focus located $\sim 1.5\text{mm}$ below pellet surface). Panels C and D illustrate the ultrasound images of the same cell pellets imaged by the 40MHz transducer. Of note the specular reflection on the pellet surface using the 20MHz transducer, absent for the 40MHz transducer. Panel E illustrates the H&E staining of unexposed cells; while in panel F extensive nuclear condensation and cellular damage can be seen.

Normalized power spectra were taken by choosing the region of interest (ROI) centred approximately at the transducer focus and 1 mm in length. Details can be found elsewhere[5]. The normalized power spectra from the 40MHz transducer are plotted in Figure 2. Theoretical models can be used to relate the slope to an effective scatterer size[4]. The spectral slope for the 0h timepoint (0.28dB/MHz) predicts an effective scatterer radius of $6.3\mu\text{m}$. The spectral slope for the 20MHz (0.81dB/MHz) predicts an effective scatterer radius of $7.2\mu\text{m}$, in reasonable agreement with the measured radius of $5\mu\text{m}$. No corrections were made for the intervening tissue attenuation nor attenuation within the analysis window, which would have increased the slope and reduce the effective scatterer size.

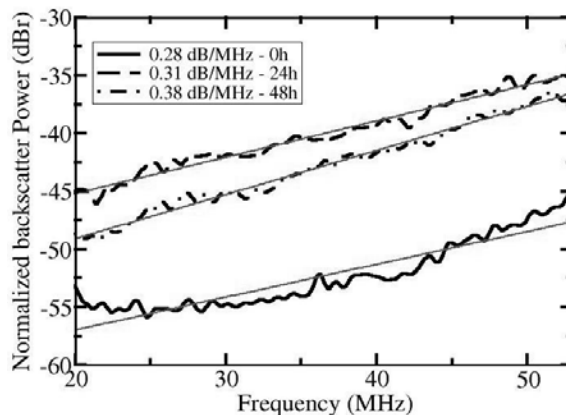


Figure 2: Normalized power spectra of AML cells (solid) and cells exposed to cisplatin for 24h (long dash) and 48h (dot dash), representing an average of 120 independent locations within the pellet (corresponding images in figures 1A and 1B).

To better visualize the contrast that may be anticipated when untreated tissues are adjacent to treated tissues, a three-layer pellet was created. The first (bottom) layer of the pellet contained unexposed cells, the second (middle) layer 24h cisplatin exposed cells and the third (top) layer unexposed cells. Figure 3A and 3B show the images collected using the 20MHz and 40MHz transducers, respectively. The treated layer of cells can be clearly differentiated from the untreated. With the 40MHz transducer the bottom layer could not be visualized due to the attenuated ultrasound. The histology of the pellet corresponded well with the ultrasound images.

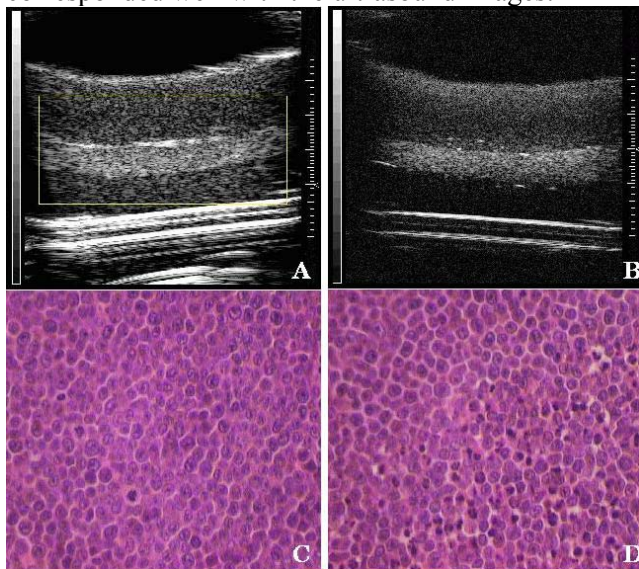


Figure 3: Ultrasonic images of a three layer AML pellet (normal-treated-normal) using the 20MHz (A) and 40MHz (B) transducers. The treated layer can clearly be differentiated due to the backscatter increase (~11dB). H&E stains of the pellet from the cisplatin unexposed top layer (C) and of the boundary between the unexposed top and exposed middle layers (D). The boundary between the two layers crosses the image diagonally.

In these experiments, there are several noted differences with respect our previous published data using the AML cell pellet system. First, there was no histologic or ultrasound difference between pellets exposed to cisplatin for up to 16h when compared to unexposed cells. In our previous study histologic and ultrasound differences were detected as early as 3h after exposure. Furthermore, the damage phenotype, as assessed by H&E staining (Figures 1(F) and 2(B)) is different: there is little evidence of the extended fragmentation of the nuclear material seen previously.

While the data generated by the cell culture system is very consistent within a set of experiments

performed from cells grown concurrently in culture, the same experiment repeated several weeks later might exhibit considerable variation in the kinetics of cell response and the damage phenotype. Furthermore, while the increase in backscatter is consistent with previously published values, the increases in spectral slopes measured (Fig.2) are smaller. The increased SNR of the new instrument and greater bandwidth have increased the precision of our measurements. It is unclear whether the slope changes are related to changes in scatter size or changes in the attenuation of the pelleted material. Finally, prominent features in the histology are the “empty spaces” in the pellets of the treated cells (Figures 1F, 3B). It is not known if this is an artifact of the staining procedure. If present during the imaging, these spaces may account for some of the increase in the ultrasound backscatter observed.

II. IMAGING CELL PELLETS: CELL DECAY EXPERIMENTS

To detect changes in the backscatter signal from cells that are left to decay, AML cell pellets were imaged at different timepoints while left in room temperature PBS. In this system there was no further centrifugation of cells, therefore eliminating any cell packing bias that may result from different cell properties and centrifugation.

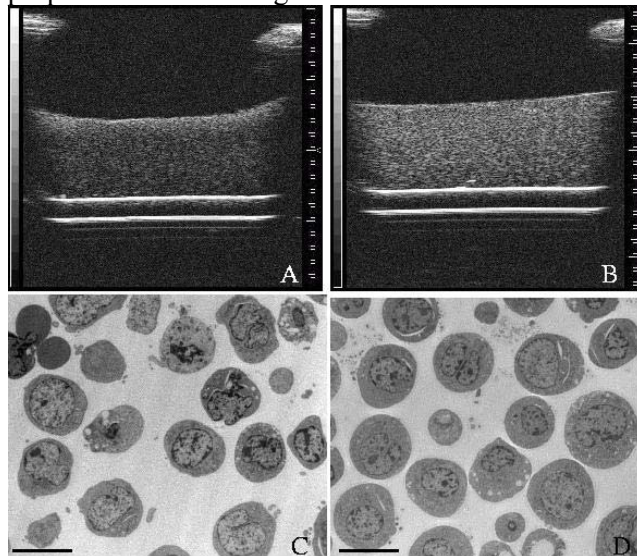


Figure 4: Ultrasonic B-mode images (8x8mm) of AML cell pellets using a 40MHz f3 transducer immediately after centrifugation (A) and after 5 hours of decay (B). Electron micrographs of normal AML cells (C) and cells taken from the 5h pellet (D). Bars: 10 μ m.

Figure 4 illustrates the change in backscatter for an AML pellet imaged with a 40MHz f3 transducer (diameter 3mm) immediately after the centrifugation (A) and five hours later (B). The measured increase in the midband fit after 5 hours was ~ 6 dB. In separate experiments and after 30 hours, the increase in the midband fit was ~ 11 dB (data not shown). Changes in the cell morphology are shown in Figures 4C (normal AML cells) and 4D (5 hour decay). The cells swell, increase in size and become more spherical. Other changes include the presence of small vacuoles in the cytoplasm and subtle changes in nuclear morphology, features typical of an oncotic cell death.

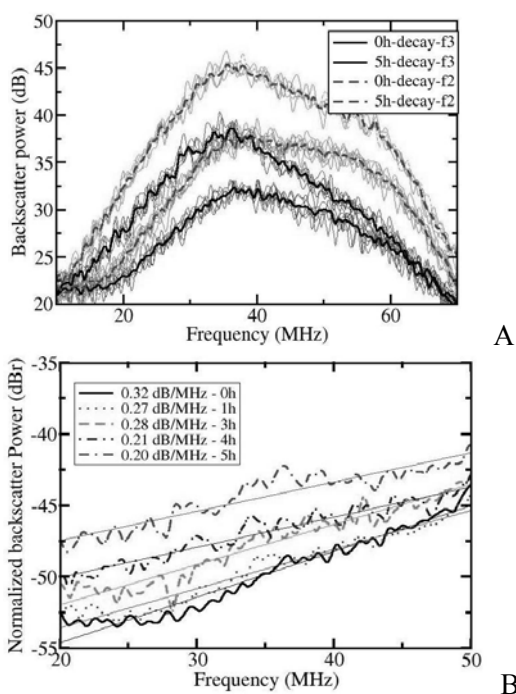


Figure 5: Ultrasonic spectra from a 1mm ROI centered at the transducer focus. In panel A) the data were collected from same pellets using the f2 (dashed) and f3 (solid) 40MHz transducers for 0 and 5h hours after pelleting. Faint lines represent the averages of 30-40 locations within a scanning plane. B) The normalized averaged data from the f3 transducer 0,1,2,3,4 and 5 hours after pelleting. The slopes are included in the inset.

The non-normalized and normalized power spectra for this decay experiment are shown in Figure 5A and 5B, respectively. In figure 5A the power spectra for the pellets at 0h and 5h are shown, for the f2 40MHz transducer (dashed lines) and the f3 40MHz transducer (solid lines). The thick lines represent the average of 5 planes of data (at least 30 independent locations per plane and each plane average is shown as light thin lines about the average).

Apart from the increase in the mid-band fit, the most striking feature is the change in slope of the normalized power spectra. As the scatterer becomes larger, a decrease in the slope of the normalized power spectra is predicted. Figure 5B illustrates that this change is gradual with time. Fitting the slope data to theoretical predictions, an effective scatterer radius for the normal AML cells is calculated as $5.5 \mu\text{m}$ and $7.7 \mu\text{m}$ for the 5-hour timepoint. The backscatter increase may be due to the increase in scatterer size.

III. IMAGING SINGLE CELLS

Improvements in transducer technology have recently enabled us to detect backscatter from single cells in dilute solutions. Analysis of the backscatter from single cells will allow us to answer some questions critical to understanding the nature of the changes in backscatter intensities observed following changes in cell structure. To assess the accuracy of the single-cell detection technique, we first examined the backscatter from polystyrene (PS) microspheres.

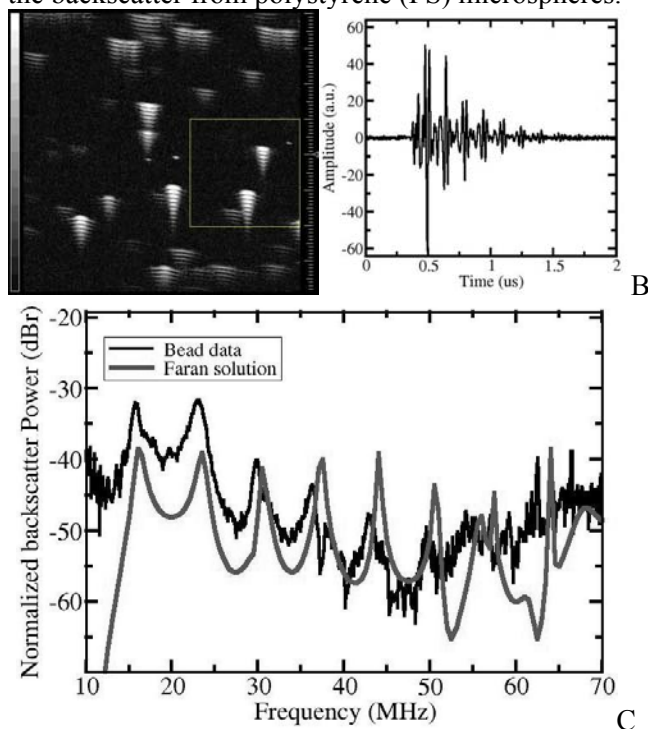


Figure 6: (A) Ultrasonic B-mode image (8x8mm) of $43 \mu\text{m}$ diameter polystyrene microspheres (B) A representative bead backscatter rf line acquired. (C) Power spectra of the bead backscatter compared to Mie scattering theory (based on the Faran-Hickling solution). Note that the theoretical curve was *not* scaled *nor* translated.

These microspheres can support shear waves, and thus, depending on the ka value, can produce resonance-rich power spectra.

An example of imaging a $43\mu\text{m}$ polystyrene microsphere solution is shown in figure 6(A). While the original pulse is a short duration (one and a half cycle) broadband pulse, the returned signal is protracted due to the resonance pattern excited, producing the striking images. In figure 6(B) the backscatter from one single sphere is plotted. A comparison of the power spectra from the $43\mu\text{m}$ beads (averaged over ~ 20 scattering events) to analytical solutions of the Faran-Hickling model (using polystyrene density of 1.06 g/mL , speed of sound 2350 m/s and Poisson's ratio 0.35) shows good agreement in the locations of the resonant peaks. It should be noted that there was neither scaling nor translation of the theoretical data in Figure 6C. This instilled a reasonable level of confidence in the analysis of the backscattered signals of the individual scatterers and their frequency spectra.

We are currently in the early stages of the comparative analysis of backscatter from single cells and cell ensembles (cell pellets) but some interesting features have already been observed. Figure 7(A) illustrates a typical image of a more dense solution of AML cells, as shown on the VS40B instrument. We can control the cell volumetric density in the solution and thus collect many individual scattering events for averaging. Figure 7(B) illustrates the backscatter from a single AML cell (diameter $\sim 10\mu\text{m}$) compared to the original pulse (reflection off a quartz plate, scaled) and the *non-scaled* backscatter from a $10\mu\text{m}$ PS microsphere. The backscatter from the cell is longer than the original pulse, and the frequency content differs. This is shown in figure 7(C) in which the power spectra from the AML cells, the $10\mu\text{m}$ PS beads and the quartz plate (translated along the y-axis by $\sim 52\text{dB}$) are plotted. There is a $\sim 7\text{MHz}$ shift in the peak of the power spectrum between the cell, PS bead backscatter and the quartz plate reflection. Furthermore, at 70MHz there is a strong peak in the bead power spectrum, well beyond the bandwidth of the 20MHz transducer. The location of the peak corresponds to the first resonant peak in the Faran-Hickling formulation. No such peak is detected in the cell backscatter. The mention of resonance from cell backscatter in the proceedings abstract was erroneous, as impedance mismatches between the front end of the transducer and the pulser produced odd pulses

that were interpreted as a features of what was imaged. This has now been corrected.

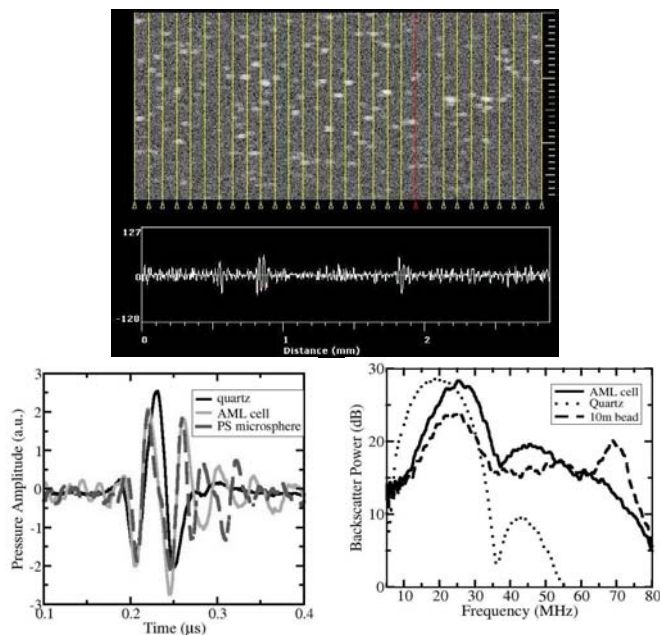


Figure 7: (A) Demonstration of backscatter from individual cells. (B) Comparison of typical backscatter from an AML cell, a $10\mu\text{m}$ diameter PS microsphere and a quartz plate reflection (scaled to match backscatter amplitude from cells and beads). (C) Comparison of averaged power spectra from cells, PS beads and the quartz plate (scaled).

It is somewhat surprising that the backscatter amplitude from a $10\mu\text{m}$ diameter PS microsphere is comparable to that of a cell if one considers acoustic impedance differences: while its' density is slightly less, the speed of sound is considerably greater. Slight variations in the radius of the AML cell and the large sensitivity to scatterer radius may account for this part of this, however, in that particular experiment we rarely measured cells with radius greater than $10\mu\text{m}$.

In dilute suspensions, the backscatter from untreated AML cells is greater than the backscatter from treated AML cells (data not shown). This was not anticipated, and is the opposite of what one might expect given the results of Figure 1, as we have hypothesized that nuclear condensation of the treated cells may account for part of the backscatter increase. This result has two interpretations: either the packing of the cells account for most of the increase in backscatter seen in our cisplatin experiments, as hypothesized by Hunt et. al.[6], or the nature of the backscattering process has been altered in single cell experiments. It is possible that while cells are packed

in the pellet, the interface with the largest acoustic impedance mismatch is the cytoplasm/nucleus boundary (as the cell pellet is a continuum, see Figure 1(E)), whilst in solution it becomes the solution/cell membrane boundary.

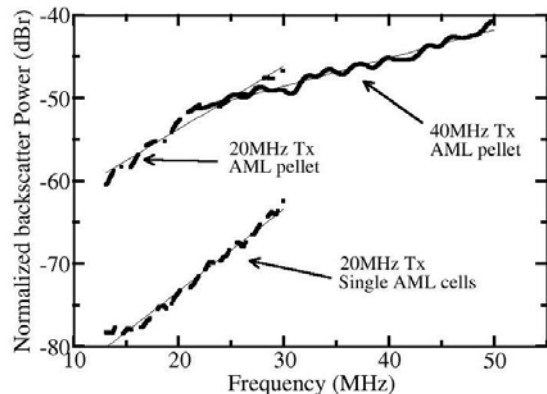


Figure 8: Comparison of the normalized backscatter power spectra for pellets and for single cells.

Finally, a comparison of the normalized spectra of individual cells vs. that of pellets is shown in Figure 8. The slopes calculated when using the 20MHz transducer (in the 0.7-0.8 dBr/MHz range) is greater than that calculated when using the 40MHz transducer (in the 0.26-0.35 dBr/MHz range), as predicted theoretically[4]. The slopes for single cells in solution are slightly greater, even though more data need to be collected. Moreover, the mid-band fit decreases by about 20dB when comparing the spectra from single cells to pellets. As this implies an intensity change on the order of 100, and the backscatter from the pellet is the result of tens of thousands of cells within the resolution volume, we hypothesize cancellation occurs, implying than one cannot assume a random collection of scatterers and add their contributions to find the total backscatter for a collection of cells.

IV. CONCLUSIONS

The backscatter increase associated with cells treated with cisplatin can be detected at both 20MHz and 40MHz. Oncotic cell death also results in a backscatter increase, but a decrease in the spectral slope, possibly attributed to cell swelling and thus an increase in scatterer size. Our imaging apparatus has detected the backscatter from single cells, and the slopes of the normalized power spectra are similar to the ones measured by the pellets. Backscatter from

single cisplatin exposed cells is less than that for untreated cells, suggesting, but not demonstrating, that cell packing (scatterer distribution) may have a significant effect in the backscatter. Finally, for polystyrene microspheres of dimensions similar to biological cells (10-40 μm), resonant spectra can be detected that are in good agreement with theory.

ACKNOWLEDGEMENTS

The authors would like to acknowledge the financial support of the Canada Foundation for Innovation, the Whitaker Foundation, the Canadian Institutes of Health Research, the Natural Sciences and Engineering Research Council of Canada, and the Ontario Innovation Trust.

REFERENCES

- [1] G. J. Czarnota, M. C. Kolios, H. Vaziri, S. Benchimol, F. P. Ottensmeyer, M. D. Sherar, and J. W. Hunt, "Ultrasonic biomicroscopy of viable, dead and apoptotic cells," *Ultrasound Med Biol*, vol. 23, pp. 961-5, 1997.
- [2] M. C. Kolios, G. J. Czarnota, M. Lee, J. W. Hunt, and M. D. Sherar, "Ultrasonic spectral parameter characterization of apoptosis," *Ultrasound Med Biol*, vol. 28, pp. 589-97, 2002.
- [3] R. Baddour, M. D. Sherar, G. J. Czarnota, J. W. Hunt, L. Taggart, A. Giles, N. R. Farnound, and M. C. Kolios, "High frequency ultrasound imaging of changes in cell structure including apoptosis," *Proceedings of the IEEE Ultrasonics Symposium*, pp. 1639-1644, 2002.
- [4] F. L. Lizzi, M. Astor, A. Kalisz, T. Liu, D. J. Coleman, R. H. Silverman, R. Ursea, and M. J. Rondeau, "Ultrasonic spectrum analysis for assays of different scatterer morphologies: theory and very-high frequency clinical results," presented at 1996 IEEE Ultrasonics Symposium, 1996.
- [5] F. L. Lizzi, M. Greenebaum, E. J. Feleppa, M. Elbaum, and D. J. Coleman, "Theoretical framework for spectrum analysis in ultrasonic tissue characterization," *J Acoust Soc Am*, vol. 73, pp. 1366-73, 1983.
- [6] J. W. Hunt, A. E. Worthington, A. Xuan, M. C. Kolios, G. J. Czarnota, and M. D. Sherar, "A model based upon pseudo regular spacing of cells combined with the randomisation of the nuclei can explain the significant changes in high-frequency ultrasound signals during apoptosis," *Ultrasound Med Biol*, vol. 28, pp. 217-26, 2002.

Corresponding author:

* M.C. Kolios, e-mail: mkolios@ryerson.ca